VECTOR MAGNETIC FIELD EVOLUTION, ENERGY STORAGE, AND ASSOCIATED PHOTOSPHERIC VELOCITY SHEAR WITHIN A FLARE-PRODUCTIVE ACTIVE REGION

K. R. KRALL

The University of Alabama in Huntsville, Ala. 35899, U..S.A.

J. B SMITH, JR.*

NOAA/SEL, Boulder, Colo. 80302, U.S.A.

M. J. HAGYARD, E. A. WEST, and N. P. CUMMINGS

NASA/MSFC, Ala. 35812, U.S.A.

(Received 26 June; in revised form 22 September, 1981)

Abstract. The evolution of vector photospheric magnetic fields has been studied in concert with photospheric spot motions for a flare-productive active region. Over a three-day period (5–7 April, 1980), sheared photospheric velocity fields inferred from spot motions are compared both with changes in the orientation of transverse magnetic fields and with the flare history of the region. Rapid spot motions and high inferred velocity shear coincide with increased field alignment along the $B_L = 0$ line and with increased flare activity; a later decrease in velocity shear precedes a more relaxed magnetic configuration and decrease in flare activity. Crude energy estimates show that magnetic reconfiguration produced by the relative velocities of the spots could cause storage of $\sim 10^{32}$ erg day^{-1}, while the flares occurring during this time expended $\lesssim 10^{31}$ erg day^{-1}.

Maps of vertical current density suggest that parallel (as contrasted with antiparallel) currents flow along the stressed magnetic loops. For the active region, a constant-α, force-free magnetic field ($\mathbf{J} = \alpha\mathbf{B}$) at the photosphere is ruled out by the observations.

1. Introduction

The energy released in a solar flare is believed to be derived from the free energy stored in stressed magnetic fields. An attractive mechanism for storage is the shearing of magnetic fields due to motions at or below the photosphere where hydrodynamic forces dominate. In the upper solar atmosphere where magnetic forces are dominant over fluid motions and where the large-scale field configurations must be predominantly force-free, the field presumably accommodates the motion of its footpoints through a continuous adjustment of electric currents from one (largely) force-free equilibrium state to another. Low and Nakagawa (1975), in a two-dimensional analysis, studied the evolution of force-free fields as a function of photospheric footpoint motion. In a subsequent paper, Low (1977a) obtained analytical solutions to two boundary value problems which demonstrated the association between sheared photospheric velocity fields, the alignment of horizontal (or transverse, B_T) magnetic fields with the longitudinal neutral line (loci of $B_L = 0$), and the development toward critical conditions suggestive of flares. In a stability analysis, Low (1977b) further demonstrated that for these boundary value

* Presently located at NASA/MSFC, Huntsville, Ala. 35812, U.S.A.

Solar Physics 79 (1982) 59–75. 0038–0938/82/0791–0059$02.55.

problems, the sequence of solutions starting from a potential field is stable until the displacement of footpoints parallel to the neutral line reaches a critical value, after which the solutions become unstable. Birn *et al.* (1978) addressed the general magnetostatic problem and demonstrated mathematically the nonexistence of equilibrium solutions when the system has evolved to this critical state. Both papers interpret this critical point as the onset of flare eruption. Furthermore, Low showed that the B_L component can remain virtually unchanged throughout the evolution, a point which enhances the desirability of transverse field measurements.

Several related observational studies have investigated the relationship between the magnetic field configuration and the occurrence of flares. The transverse field component has been inferred by use of chromospheric and coronal emission structure, which are presumably aligned with the field direction and located at the levels of the energy storage and release (e.g., Tanaka and Nakagawa, 1973; Rust and Bar, 1973; Bruzek, 1975; Prata, 1972; Neidig, 1979). Prata (1972) found a significantly higher flare frequency in the case of Hα fibrils aligned parallel to the photospheric neutral line as compared to the perpendicular case. Neidig (1979) showed pre- to post-flare fibril evolution, which appeared to be associated with increased energy storage and relaxation, respectively. Until recently, direct measurements of B_T have been rare and even now are limited to the underlying photosphere, but they have indicated results similar to the above (Smith *et al.*, 1979), as well as 'anomalous' transverse structure as being associated with flare productivity (Severny, 1964).

In this paper these relationships are explored further for an active region (NOAA 2372) which was characterized by very rapid growth and development, significant photospheric motions, and high flare activity from 5 to 7 April, 1980. The analysis emphasizes the evolution of the region's vector magnetic field, as observed with NASA Marshall Space Flight Center's (MSFC's) vector magnetograph, and the relation of this field to the sunspot proper motion and flare history of the region. In Section 2, we discuss the observational data base of vector field measurements, Hα flare history, flare locations, and white light sunspot motions during the period. In Section 3, we discuss the possible energy budget and estimate the electric currents driven by the magnetic field. These results are summarized in the discussion in Section 4.

2. Observations

Active region 2372 was born on 4 April in the northeast quadrant, very near a large and somewhat complex region which had rotated onto the visible disk a few days earlier. AR 2372 developed rapidly in magnetic field strength, field gradients, and magnetic complexity; within 24 to 36 hr, the region was described as a magnetic beta-gamma (somewhat complex) spot group with a delta configuration (umbrae of opposite polarities within a common penumbra) and had produced its first large flare (an M5/1B at 5/15 : 54 UT). The MSFC magnetograph obtained several sets of vector data of the region from 5 to 11 April. Because of the proximity to disk center during the period of interest ($\approx$ east 25° at 5/13 : 34 to west 7° at 7/19 : 00), longitudinal and transverse field components are here assumed to be vertical and horizontal, respectively.

2.1. Observational technique

The MSFC vector magnetograph employs a tunable 0.0125 nm bandpass Zeiss filter together with electro-optical modulators to obtain integrated Stokes intensities in the Fe I 525.02 nm absorption line. For details of the system see Hagyard *et al.* (1981). For such a magnetograph system, strong magnetic fields ($\gtrsim 2000$ G) may be estimated by tuning the filter bandpass through the Fe line or by calibrations obtained from the relevant radiative transfer equations (Hagyard, 1970). However, this paper focuses on the field configuration in the vicinity of a neutral line dividing a relatively weak positive spot from surrounding weak negative penumbra and umbrae. Thus the 'weak field' approximations to the radiative transfer solutions (Bray and Loughhead, 1964) are used in this paper:

$$B_L = B \cos \Psi = C_1(\Delta\lambda) P_V(\Delta\lambda) ,$$
$$B_T = B \sin \Psi = C_2(\Delta\lambda) [P_Q(\Delta\lambda)]^{1/2} . \quad (1)$$

In these equations Ψ is the angle between the vector field **B** and the vertical direction, $\Delta\lambda$ refers to the wavelength offset from line center, and $P_V(\Delta\lambda)$ (or $P_Q(\Delta\lambda)$) is the fractional circular (or linear) polarization measured at the filter position $\Delta\lambda$ and integrated over the filter bandpass. The constants C_1 and C_2 are derived from theoretical calibration curves of $P_V(\Delta\lambda)$ and $P_Q(\Delta\lambda)$ as functions of B. These theoretical curves are computed using the solutions to the coupled transfer equations for the Stokes parameters as derived by Kjeldseth Moe (1968). Assuming the line-formation mechanism of pure absorption, LTE and a homogeneous magnetic field, integral representations for the Stokes parameters are numerically evaluated using the penumbral atmospheric model of Kjeldseth Moe and Maltby (1969). The resulting emergent V and Q Stokes intensities are then computationally averaged over the Zeiss filter transmission profile to produce $P_V(\Delta\lambda)$ and $P_Q(\Delta\lambda)$. For field strengths less than 10^3 G, we find that Equations (1) are valid within ± 100 G. Consequently, from magnetograph measurements of $P_V(\Delta\lambda)$ and $P_Q(\Delta\lambda)$, the field intensity B (averaged over the magnetograph spatial resolution of $\simeq 2.5$ arc sec) and departure from vertical Ψ can be calculated. The azimuth ϕ of B_T is calculated from the relative intensities of linear polarizations measured in two independent coordinate systems at (0°, 90°) and ($\pm 45°$) to the magnetograph's analyzer axis. Appendix I is a discussion of the effects of Faraday rotation, suggesting that it does not materially alter the results of these observations

2.2. Spot motions

Figure 1 shows the evolution of circular polarization (related to longitudinal magnetic field strength) maps of the region for the first three days of observations. MSFC white light disk patrol images were used to measure spot positions for the five-day period starting mid-day on the 5th. Significant spot motions occurred only within the first two days, with the negative follower (F1) and negative delta spot (F2) migrating eastward and the isolated leading (positive) polarity (L2) and negative (F3) moving westward relative to the leader (L1) (see Table I); these spot motions indicate shearing of the photospheric velocity field took place. Figure 1 shows that the longitudinal field evolution

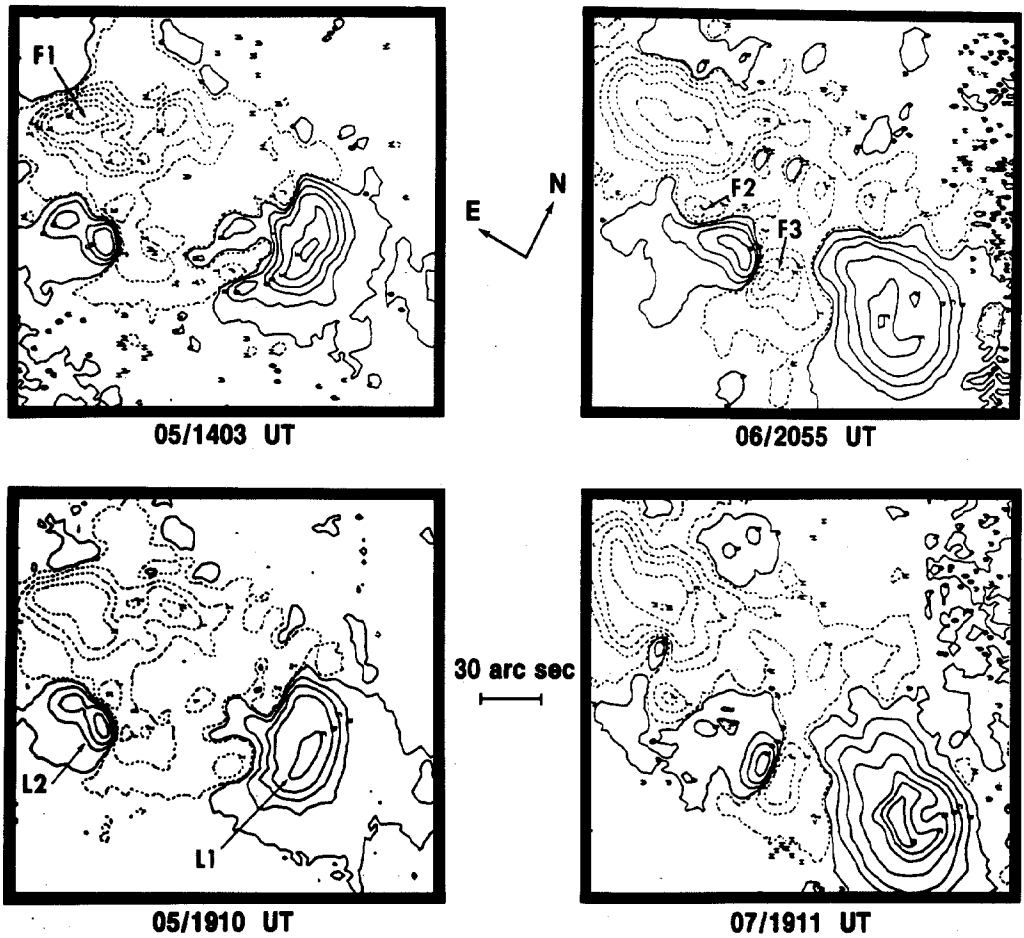

Fig. 1. Contours of circular polarization measurements for AR2372 during the time of spot motions and greatest flare activity. In all figures, solid lines depict positive magnetic polarity, dashed lines are negative, and orientations are the same. Contours levels are ± 0.01, 1.0, 2.5, and multiples of $\pm 5\%$ polarization.

mirrored these observed spot motions. From 14:06 UT on 7 April to 13:18 UT on 10 April, no measurable motions were seen.

2.3. Flare History and its Relationship to Magnetic Fields

Figure 2 depicts the occurrence of X-ray flares in the region together with the X-ray class, as explained in the caption. One X2, eight M and numerous C class flares occurred during the period covered in Figure 1, in which all significant spot motions occurred. By the time of the two-ribbon M5/1B flare shown in Figure 3a (maximum at 5/15:54 UT) the delta configuration had developed in the south central portion of the region. This flare and the homologous X2/1B flare of 6/14:27 UT) (Figure 3b), which were both accompanied by moderately large, discrete frequency, centimetric radio responses and by dark surge material emanating from the trailer spot, are seen to be strongly associated with

TABLE I

Average shear-producing spot velocities (m s^{-1})[a]

Spot	From 5/13 : 34 to 6/15 : 12 UT	From 6/15 : 12 to 7/14 : 06 UT
F1	$+75 \pm 40$	$+220 \pm 50$
L2	-160 ± 40	0 ± 50

[a] Positive and negative denote eastward and westward motion, respectively.

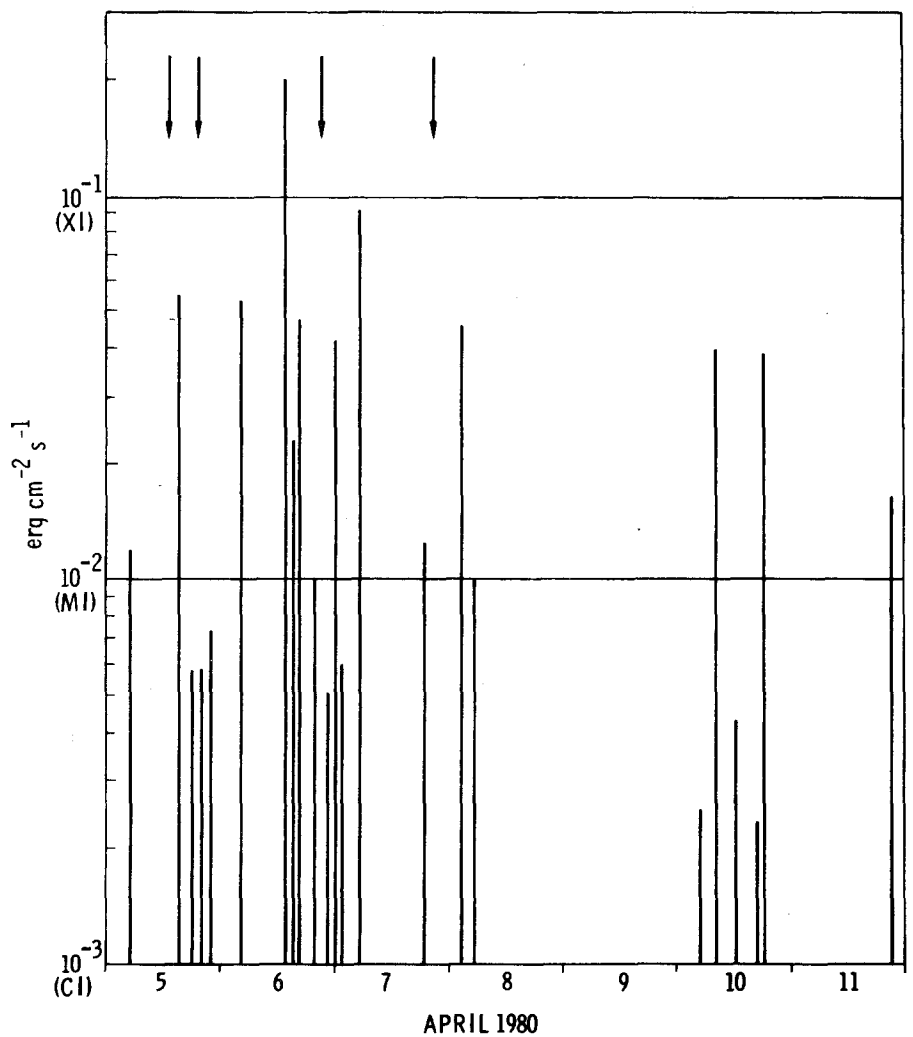

Fig. 2. Peak 1–8 Å intensity vs time of flare maximum for the X-ray flares of the first seven days of AR2372. In the text, numbers following C, M, and X indicate multiples of 10^{-3}, 10^{-2}, and 10^{-1} erg cm^{-2} s^{-1}, respectively. From preliminary report of NOAA SMM support group.

the isolated positive pole (L2) and its northern- and leading-edge neutral line. In addition, of six locatable Hα flares (via *Space Environment Service Center primary reports*) on 5 April, the two class M's and at least one class C occurred within one heliographic degree of the isolated pole. Two others occurred along the intrusion of negative polarity F3 into the area of the positive leader (Figure 3a). With one possible exception, all the identifiable flares of 6 April were centered near the isolated pole (L2), including an M5/1B at 04 : 13 UT which was accompanied by type II and IV bursts and photospheric white light enhancement. The intrusion of negative polarity into the positive leader had simplified by 14 : 36 UT (Figure 3b), although isolated elements of later flares (and the X2/1B) occurred in this area.

The longitudinal (contours) and transverse (line segments) magnetic field components at 5/16 : 03 UT, nine minutes after the M5 flare maximum, are shown in Figure 4a; the boundaries of the brightest off-band Hα patches near flare maximum are also shown

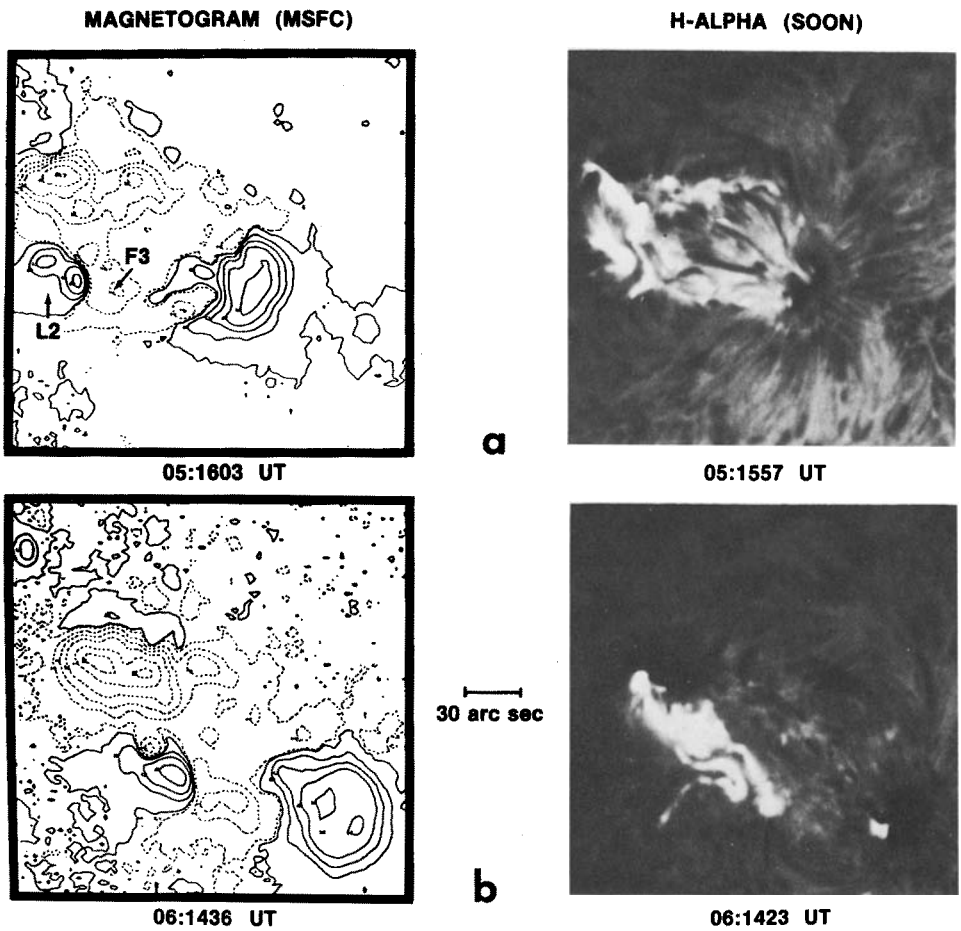

Fig. 3. Magnetograms and Hα images for two flares: (a) M5/1B on 5 April and (b) X2/1B on 6 April. Note the two ribbon structure across the neutral line of isolated pole L2.

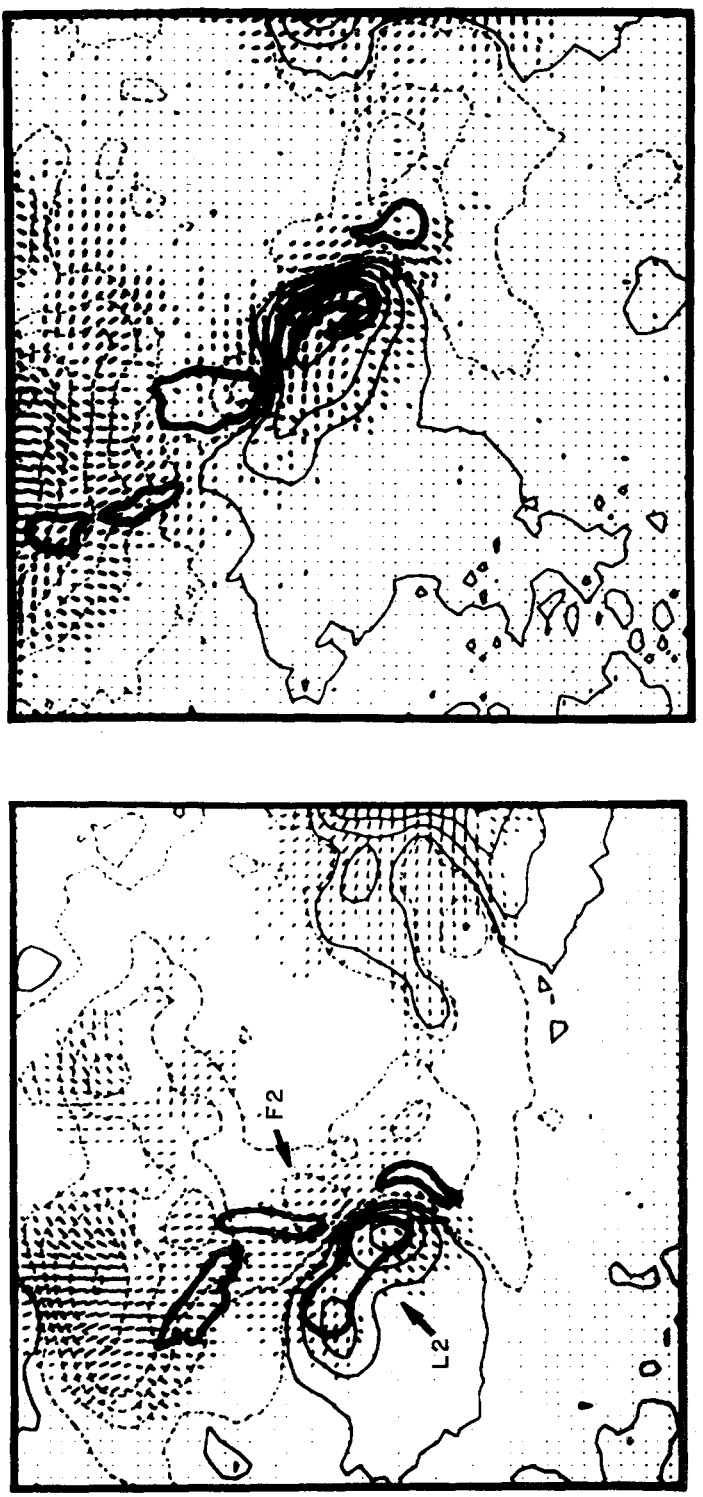

Fig. 4. Superposition of Hα emission (bold contours) on circular polarization (thin-lined contours, proportional to longitudinal magnetic field in vicinity of isolated pole) and linear polarization measurements (line segments parallel to and with lengths proportional to transverse fields in vicinity of isolated pole). (a) M5 on 5 April, (b) X2 on 6 April. The area shown is 2.25×2.25 arc min^2.

(bold contours). Note the Hα location and alignment of the transverse field to the neutral line separating L2 from F2. Similarly, in Figure 4b, the 6/14 : 27 UT flare emission is superimposed on longitudinal and transverse plots taken from 14 : 36 to 14 : 50 UT, nine minutes after maximum. Deteriorating observing conditions made field measurements questionable throughout the flare time period, although the sheared appearance and flare-element locations are similar to those of the previous flare.

The region's growth slowed on 7 April although longitudinal gradients along the isolated pole had not appreciably weakened by 19 : 10 UT. Except for an M8 at 7/05 : 33 UT and an M5 at 8/03 : 10 UT, flare activity declined substantially over the next 48 hr. Although there was increased flaring on 10 April, including a spectrally hard M4 event at 09 : 22 UT, foreshortening seriously impaired magnetic field measurements and proper motion analysis. Thus, the lack of apparent spot motions on that day and the previous day is inconclusive.

2.4. Transverse field evolution

Figure 5 shows a sequence of enlarged magnetograms in the area surrounding the isolated pole (L2 of Figure 1). When first observed, two hours before the M5 flare on 5 April, a fanning out of the transverse field could be seen along the leading edge of the positive spot (Figure 5a). Along the northern section of the neutral line of L2 the azimuthal

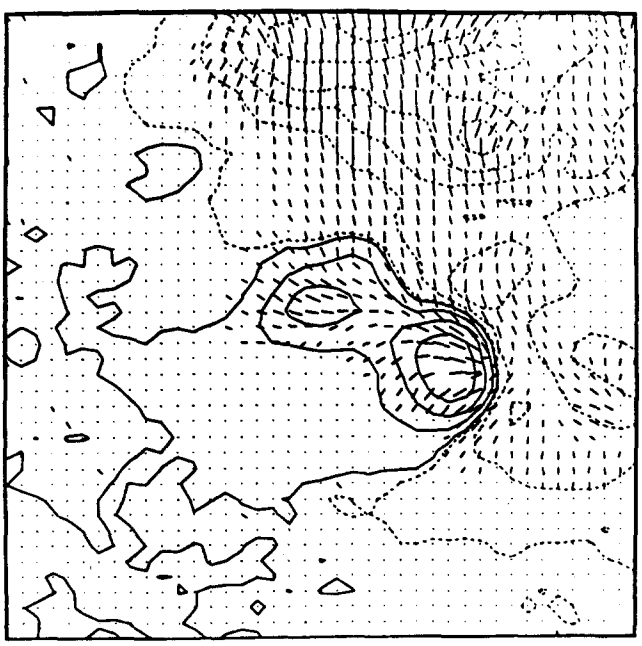

Fig. 5a.

Fig. 5a–c. Field development during the westward migration of the isolated positive spot. The area shown is 1.67 × 1.67 arc min^2.

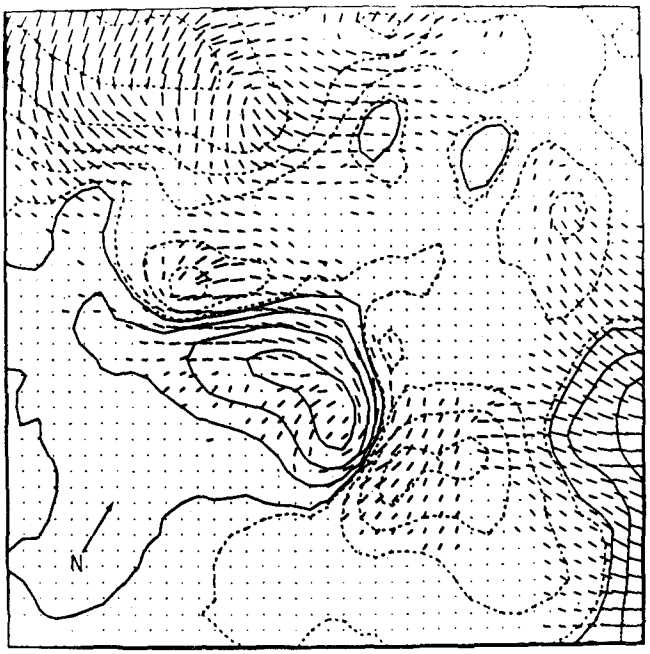

APRIL 6 2055 UT

Fig. 5b.

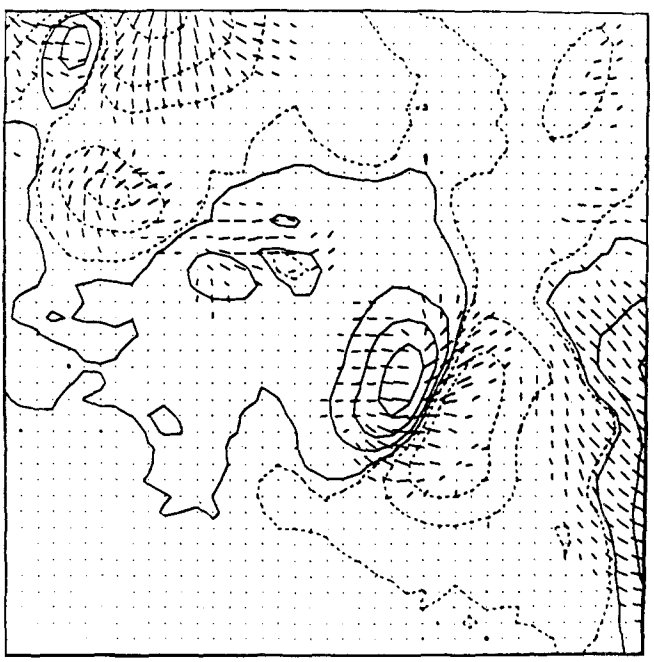

APRIL 7 1910 UT

Fig. 5c.

orientation was inclined at various angles to the neutral line. On 6 April, during and after the period of greatest absolute motion of L2 and its largest velocity shear with respect to F1 and F2, the transverse field direction along their common neutral line exhibited a significant reorientation, with the azimuthal direction being nearly parallel to the neutral line along its full extent (Figure 5b). Horizontal fields along the leading edge had lost their fanned out appearance, in favor of similar alignments with the neutral line, indicating that loops connecting footpoints on opposite sides of the neutral line were twisted so as to be nearly along (rather than perpendicular to) the line. Sufficiently time-resolved observations from 14 : 00 to 21 : 00 UT, during which four major flares occurred, showed no evidence of significant change in the transverse field orientations. However, by 19 : 10 UT on 7 April (Figure 5c) some 23 hr after the isolated pole's motions had ceased, the transverse component along its leading edge had regained a more 'relaxed' orientation with the azimuths directed more normal to the neutral line. Also, at this time the components along the northern and trailing edge had weakened and appeared less stressed than previously.

The evolution of the transverse field exhibited in Figure 5 may be interpreted in terms of fluid motions inferred from the white light spot motions. In this picture, the observed reorientations developed when the footpoints of the original loops of closed field lines connecting opposite polarities (L2 and surrounding negative fields) were swept past each other by the sheared photospheric velocity pattern.

It would be interesting to compare the evolution of the transverse measurements with that of overlying Hα fibril structure. Unfortunately, available Hα patrol film does not easily lend itself to such an investigation. However, at least during the post-flare phase of the 6 April X2 event (15 : 18 UT), fibrils did appear to align closely with the neutral line along the leading (western) edge of L2, which is consistent with the transverse field orientation shown in Figure 5b. On the northern edge, the orientation of longer fibrils was more or less normal to the neutral line in contrast to the orientation of the transverse photospheric field shown in Figure 5b. Perhaps the orientations of these longer and (presumably) higher features are less influenced by motions at the photosphere level. If they trace field lines, then we can infer that the horizontal component of the field developed a variation of shear with height between 5 April and 6 April, enhancing the site's potential for field interaction and energy release.

3. Analysis

3.1. Estimates of magnetic energy build-up and flare energy requirements

For the period of analysis, we wish to compare the flare energy output to a crude estimate of the quasi-static build-up of total energy within a force-free configuration subject to horizontal shearing motion. Utilizing the vector magnetic field data is not within the scope of this work, but will be done in a later paper. Following Tanaka and Nakagawa (1973), the change in magnetic energy within a volume V enclosed by surface S can be

expressed as

$$\frac{\partial}{\partial t}\int_V \frac{|B|^2}{8\pi}\,dx\,dy\,dz = \frac{1}{4\pi}\int_S [(\mathbf{v}\times\mathbf{B})\times B]\cdot d\mathbf{s}\,, \tag{2}$$

where Joule dissipation is ignored and $d\mathbf{s}$ is the surface element. To represent the shear within a simple bipolar configuration similar to that of the delta in Figure 1, we consider a periodic constant-α force-free field with flux concentrations (spots) centered at $y = \pm(L/2)$, and $x = 0$:

$$B_z = -B_0 \sin\left(\frac{\pi y}{L}\right)\cos\left(\frac{\pi x}{L}\right)\exp\left[-(k^2-\alpha^2)^{1/2}z\right], \tag{3}$$

$$B_x = -B_0\left(\frac{L}{2\pi}\right)\left\{(k^2-\alpha^2)^{1/2}\sin\left(\frac{\pi y}{L}\right)\sin\left(\frac{\pi x}{L}\right) - \right.$$

$$\left. - \alpha\cos\left(\frac{\pi y}{L}\right)\cos\left(\frac{\pi x}{L}\right)\right\}\exp\left[-(k^2-\alpha^2)^{1/2}z\right],$$

$$B_y = B_0\left(\frac{L}{2\pi}\right)\left\{(k^2-\alpha^2)^{1/2}\cos\left(\frac{\pi y}{L}\right)\cos\left(\frac{\pi x}{L}\right) + \right.$$

$$\left. + \alpha\sin\left(\frac{\pi y}{L}\right)\sin\left(\frac{\pi x}{L}\right)\right\}\exp\left[-(k^2-\alpha^2)^{1/2}z\right],$$

where L is the characteristic size of the dipole, estimated from the observations to be 2.5×10^4 km, $k = (k_x^2 + k_y^2)^{1/2} = 2\pi/L$, and $B_0 \simeq 1500$ G is a characteristic longitudinal field for each of the opposite poles. We approximate the photospheric velocity field, crudely, as

$$v_x = \frac{v_0}{2}\sin\frac{\pi y}{L}, \qquad v_y = 0\,, \quad \text{and} \quad v_z = 0\,, \tag{4}$$

where $v_0 = 220$ m s^{-1} (Table I). Substitution into Equation (2) then gives (after cancellation from opposite vertical surfaces at $x = \pm L/2$ and at $y = \pm L$ and zero contribution from $z = \infty$):

$$\frac{\partial}{\partial t}\int\frac{|B|^2}{8\pi}\,dV = \frac{1}{4\pi}\int_{y=-L}^{L}\int_{x=L/2}^{L/2} dy\,dx(v_x B_x B_z)_{z=0}$$

$$= \frac{v_0 B_0^2 L^3}{12\pi^3}(k^2-\alpha^2)^{1/2}$$

$$\simeq 5\times10^{32}\sin\gamma \text{ erg day}^{-1}\,, \tag{5}$$

where $\sin\gamma = [(k^2-\alpha^2)^{1/2}]/k$, and γ represents the angle between the azimuthal direction of the magnetic field at the neutral ($B_z = 0$) line and the neutral line itself. The values

of γ obtained from the vector data ($\simeq 10-50°$) are appropriate only at the lower layer of the energy storage volume; in addition, the geometric assumptions used in deriving Equations (3) and (4) lose validity during the evolution. Thus, the value given in Equation (5) can only crudely be compared with the energy release requirements of the region's several flares during the time period.

Soft X-ray emission and Hα spatial information can be used to roughly estimate energy storage requirements for the flares of the period. Energy released in the soft X-ray waveband (1–8 Å) was estimated for each flare by multiplying its peak power by the time interval between half-power points. Several authors have attempted to measure the spectral distribution of radiation in flares (e.g., Canfield, 1980; Smith and Gottlief, 1973; Lin and Hudson, 1976). Canfield (1980), for an X1 and Smith and Gottlief (1973) for a 3B find the ratio of total emission so that in the 2–8 Å band to be approximately 35 and 27, respectively. There are lower limits, since the measurements were close to flare maximum, when spectral hardness normally peaks. If the appropriate value is 30, we calculate total radiative output from the flares of region 2372 to be 2.3, 9.8, and 3.6×10^{30} erg day^{-1} for 5, 6, and 7 April 1980, respectively. Mechanical energy output can vary considerably from flare to flare, and can dominate radiative output in some cases (Webb, 1980). Although the flares of this time period do not appear to be in this class, a comparable amount of mechanical and radiative energy is reasonable to expect. The resulting total output values are of the order of 10^{-1} of the storage capacity indicated by Equation (4). Even with the uncertainties involved, significant additional dissipation (e.g., non-flaring active region heating via excitation of collisionless tearing modes or current-driven instabilities) could be accommodated within such an energy budget.

3.2. Electric Current Density from Transverse Field Measurements

In principle, knowledge of the horizontal distribution of the transverse components of the magnetic field allows calculation of the vertical current density:

$$J_z = \partial B_y/\partial x - \partial B_x/\partial y)/\mu_0 ,$$

where J_z is in units of A m^{-2} and $\mu_0 = 1.2 \times 10^{-2}$ G m A^{-1} is the permeability in free space. In practice, the problem of determining spatial derivatives of the rather uncertain transverse component is compounded by the 180° ambiguity in direction inherent in any determination based upon measuring the state of linear polarization of the emergent radiation. Appendix II describes the methods used to eliminate such ambiguity. Figures 6a and 7a show the longitudinal field for the delta region on 6 and 7 April, while Figures 6b–c and 7b show electric current patterns resulting from the following approximation to Equation (6):

$$J_z(x, y) = \{[B_y(x + \Delta x, y) - B_y(x - \Delta x, y)]/(2\Delta x) - \\ - [B_x(x, y + \Delta y) - B_x(x, y - \Delta y)]/(2\Delta y)\}/\mu_0 \qquad (6)$$

(where $\Delta x = \Delta y$ is the pixel size), and was then averaged over 2 by 2 pixels (5 by 5 arc sec). A series of five J_z plots was obtained between 19 : 08 UT and 21 : 00 UT on

6 April, Figure 6b and c being the first and last of that series. Neither variations greater than those shown nor evidence of evolutionary-type change is present in the series. Note the tendency for J_z to change sign (positive = upward, negative = downward) when crossing the neutral line surrounding the positive pole. This is consistent with currents flowing along loops with footpoints on either side of the neutral line. In addition, the sense

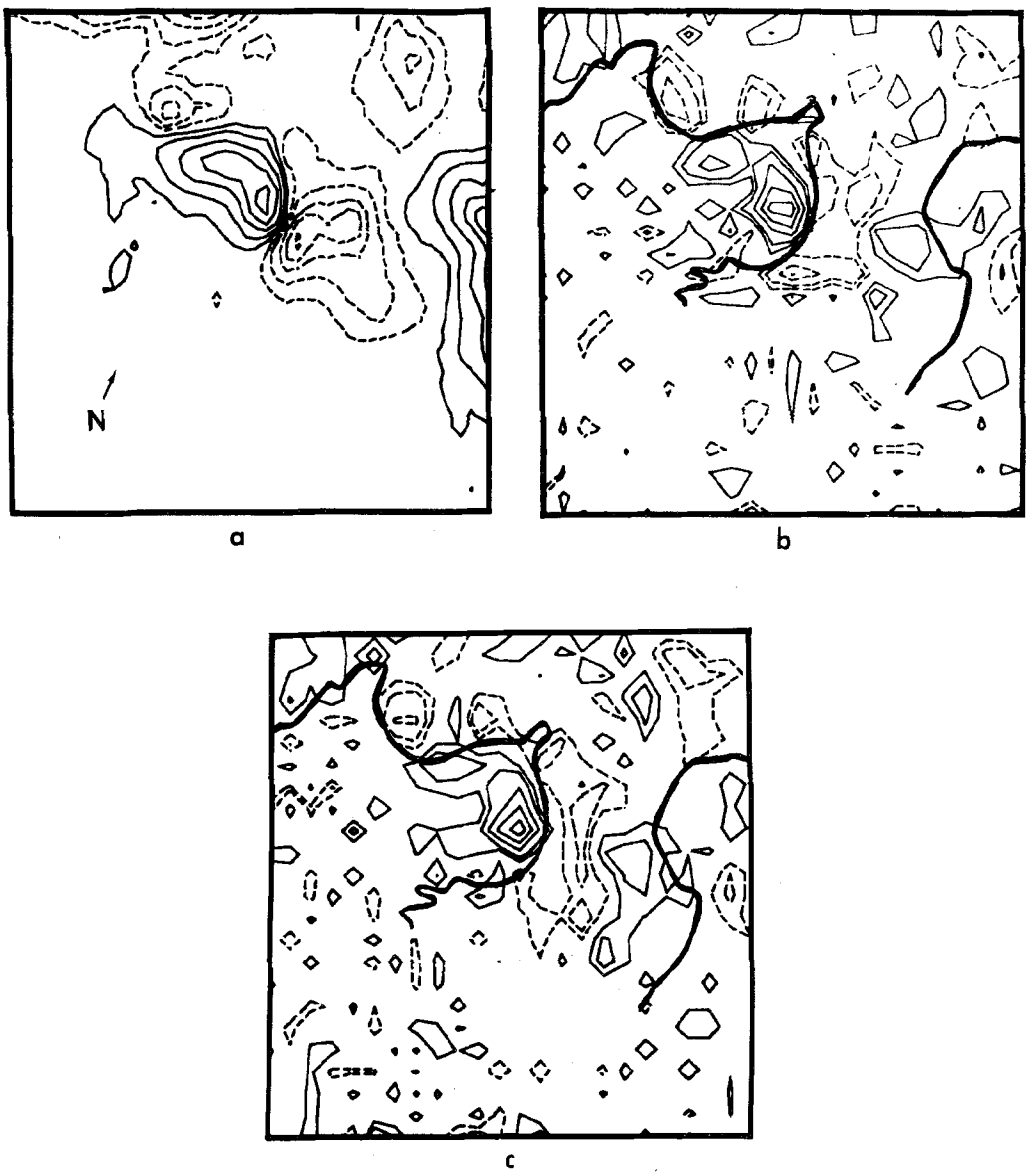

Fig. 6. (a) Longitudinal fields at 6/19:08 UT and vertical electric current density at (b) 6/19:08 and (c) 6/21:00 UT. Bold-faced line indicates longitudinal neutral line, contour levels of current density are ± 1.15 (= noise level) and multiples of $\pm 2.3 \times 10^{-3}$ A m^{-2}. The area shown is 2×2 arc min^2, consisting of 24×24 pixels.

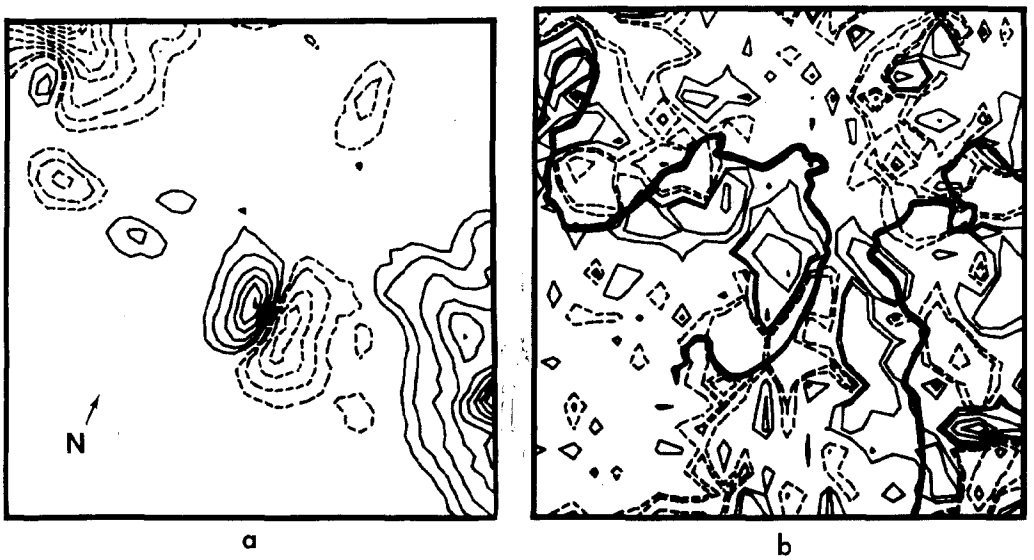

Fig. 7. (a) Longitudinal fields and (b) current density at 7/19 : 10 UT. Scale is the same as for Figure 6.

of J_z, especially along the northern extent of that neutral line, is that expected from the velocity shear. I11-defined, although somewhat anti-parallel, currents are suggested ahead (to the west) of the isolated positive pole, where horizontal compression rather than shear is more likely. Changes are clearly visible one day later (Figure 7), although major features have been conserved. Large values in strong umbral field regions (lower right and upper left) can probably be attributed to non-applicability of the weak field approximation and/or Faraday rotation effects in the data. Plots of $\alpha(=J_z/B_L$, not shown here), although retaining a predominant sense for relatively large areas ($\simeq 1$ arc min^2), cannot be considered constant. Levine (1976) found evidence for anti-parallel currents and non-constancy of α over larger scales when comparing results of extrapolated constant-α calculations to EUV and soft X-ray emission features. Sakurai (1981), employing a Green's function solution to investigate various current distributions within bipolar configurations, found that storage capacity was greater for systems characterized by parallel (rather than anti-parallel) currents, i.e., the flare-producing areas of this study.

4. Discussion and Summary

We have presented an example of reorientation of the photospheric transverse magnetic fields during a period in which shear in the inferred horizontal velocity field and frequent, strong flare activity both occurred along a magnetic neutral line (5 and 6 April). The observed sunspot motion and field development across the neutral line surrounding isolated positive pole L2 are understandable if there were magnetic loops whose footpoint

separations increased as they participated in the inferred surface flow. The coincident increase in flare activity is consistent with a continuous and quasi-static stress build-up within the overlying magnetic fields, occasionally interrupted by explosive energy release. Relative spot motions (negative F1 and F2) are shown to have continued the following day (7 April), but because of the changed photospheric geometry, there was no longer the high velocity shear across a neutral line possessing large field gradients. The measured transverse field weakened and relaxed significantly during this period, and flare activity showed a marked decline.

Crude estimates of total flare energy output (~ 1–2×10^{31} erg for 6 April) have been compared to the magnetic energy build-up of a simple bipole experiencing horizontal shearing motion similar to that observed. The results suggest that this process could generate adequate energy for the flares of the period. Vertical current density contour maps have shown a sign pattern across the $B_L = 0$ line which indicates parallel current flowing along the loops of the stressed arcade. Vertical current densities are characteristically 5×10^3 A m^{-2} when resolved over 5 arc sec.

Emerging flux cannot be discounted as an alternate or additional flare source and trigger. AR2372 was born on 4 April and although observations were scarce, emergence of the delta spot lagged that of the main leader and trailer. Its emergence into pre-existing and oppositely directed overlying fields could have produced the rising current sheets and turbulent reconnection required by the flare model of Heyvaerts *et al.* (1977). However, emergence had declined by 6 April and the time-association of flare activity with emerging flux is not nearly as striking as with horizontal spot motions.

Considering the example offered here, it would appear reasonable to expect that overlying magnetic energy build-up due to photospheric proper motions might be most sensitively determined by analysis of vector magnetograms. Preliminary quantitative efforts are, in fact, underway (Krall and Hagyard, 1981). Transverse field evolution as described in this paper is not typical of active regions observed with the MSFC magnetograph; definitive general statements concerning frequency and relationship to flare and active region energy budgets await a more systematic review of the data. It should be noted, however, that during the reported three-day period, AR2372 was exceptional in its energy storage requirements.

Acknowledgements

The authors are indebted to J. E. Smith for photographic assistance and to Dr S. T. Wu and E. Hildner for useful discussions and careful reading of the text. Portions of this work were supported by the Air Force Geophysics Laboratory (FY71218003105) through NASA/MSFC Contract NAS8–33525 (KRK and JBS), Government Work Order H–12261B (NOAA, JBS), and the NASA SMM Guest Investigator Program. Thanks also to the USAF for use of SOON/Holloman AFB Hα patrol photographs used in the illustrations and analysis.

Appendix I: Effects of Faraday Rotation

The wavelength variation of the refractive index for different polarizations will rotate the plane of observed linear polarization ϕ away from the direction of B_T. This Faraday rotation may be significant in the MSFC magnetograph data, since they are integrals of the Stokes profiles over wavelength. The effect is increasingly important for smaller values of Ψ and for larger field strengths (i.e., when there exists a significant contribution from linear polarization perpendicular to the magnetic field within the bandwidth of the filter, Landi Degl'Innocenti, 1979). Theoretical analysis has indicated that for $B \approx 1200$ G and $\Psi \approx 70°$, errors in the measured azimuth angles at $\Delta\lambda = 0.006$ nm should not exceed 10° (West *et al.*, 1980).

To investigate Faraday rotation observationally, the azimuth ϕ was measured as a function of $\Delta\lambda$ (from 0.0 to 0.012 nm in steps of 0.001 nm) at 5 different radial distances from the center of the leading positive spot within AR2372; analysis of these data in fact revealed the expected systematic variation of ϕ with wavelength $\Delta\lambda$ (West *et al.*, 1980). However, in the sheared areas studied in this paper, the fields were more nearly horizontal and weaker ($B_L \lesssim 1500$ G). From $\Delta\lambda = 0.006$ to 0.012 nm, close examination of these areas shows that variations in ϕ greater than 10° (and as great as 25°) appear only at a few data points at the center of the isolated positive spot. Although this discrepancy acts to overestimate the maximum positive value of $(\text{curl } B)_z$ in Figure 6b and c, the general contour patterns and conclusions concerning vertical current density in Section 3.2 are similar whether determined at $\Delta\lambda = 0.006$ or 0.012 nm. Therefore we conclude that the general results of this paper, using observations at $\Delta\lambda = 0.006$ nm, are not altered by Faraday rotation.

Appendix II: Treating the Ambiguity of Direction in Transverse Field Measurements

To estimate the current density J_z from Equation (5), the 180° ambiguity in direction of (B_x, B_y) is treated with a computer algorithm which employs two criteria:

(1) that direction is chosen which has a component anti-parallel to the local gradient of the longitudinal field (i.e., field lines 'emerge' from positive polarities and 'seek' negatives), and

(2) best continuity with direction of neighboring points is sought. These criteria alone, although adequate for simple configurations, do not provide reasonable results for all situations.

For example, small-scale fluctuations in B_L produce spurious directions unless criterion (1) is applied over larger areas. When given priority, criterion (2) helps to eliminate such anomalies, but could mask just the discontinuities that interest the observer. For the 6 and 7 April data, we found that the 'objective' algorithm provided consistent results independent of whether 4, 8, or 12 nearest neighbor data points were used, and that criterion (2) overrode (1) $\approx 15\%$ of the time. For 5 April, the ambiguous nature of the divergence along the leading edge of the positive polarity was too complex to satisfactorily resolve, although J_z patterns for the rest of the area of interest resembled that of 6 April.

References

Birn, J., Goldstein, H., and Schindler, K.: 1978, *Solar Phys.* **57**, 81.

Bray, R. J. and Loughhead, R. E.: 1964, *Sunspots*, John Wiley and Sons, Inc., New York, p. 194.

Bruzek, A.: 1975, *Solar Phys.* **42**, 215.

Canfield, R. C.: 1980, ion P. A. Sturrock (ed.), *Solar Flares: A Monograph from Skylab Solar Workshop II*, Colo. Assoc. Univ. Press, Appendix A.

Hagyard, M. J.: 1970, NASA TM X–64541.

Hagyard, M. J., Cumings, N. P., and West, E. A.: 1981, NASA TM–82405.

Heyvaerts, J., Priest, E. R., and Rust, D. M.: 1977, *Astrophys. J.* **216**, 123.

Kjeldseth Moe, O.: 1968, *Solar Phys.* **4**, 267.

Kjeldseth Moe, O. and Maltby, P.: 1969, *Solar Phys.* **8**, 275.

Krall, K. R. and Hagyard, M. J.: 1981, *Bull. Am. Astron. Soc.* **12**, 899.

Landi Degl'Innocenti, E.: 1979, *Solar Phys.* **63**, 237.

Levine, H.: 1976, *Solar Phys.* **46**, 159.

Lin, R. P. and Hudson, H. S.: 1976, *Solar Phys.* **50**, 153.

Low, B. C.: 1977a, *Astrophys. J.* **212**, 234.

Low, B. C.: 1977b, *Astrophys. J.* **217**, 988.

Low, B. C. and Nakagawa, Y.: 1975, *Astrophys. J.* **199**, 237.

Neidig, F.: 1979, *Solar Phys.* **61**, 121.

Prata, S. W.: 1972, *Solar Phys.* **25**, 136.

Rust, D. M. and Bar, V.: 1973, *Solar Phys.* **33**, 445.

Sakurai, T.: 1981, *Solar Phys.* **74**, 35.

Severny, A. B.: 1964, *Izv. Krymsk. Astrofiz. Obs.* **31**, 159.

Smith, E. v. P. and Gottlief, D. M.: 1973, in W. R. Bandeen and S. P. Maran (eds.), *Proceedings of Symposium on Possible Relationships between Solar Activity and Meteorological Phenomena*, NASA SP366, p. 97.

Smith, J. B., Krall, K. R., Hagyard, M. J., Cummings, N., West, E., Reichmann, E., and Smith, J. E.: 1979, *Bull. Am. Astron. Soc.* **11**, 440.

Tanaka, K. and Nakagawa, Y.: 1973, *Solar Phys.* **33**, 187.

Webb, D. F.: 1980, in P. A. Sturrock (ed.), *Solar Flares: A Monograph from Skylab Solar Workshop II*, Colo. Assoc. Univ. Press, Appendix B.

West, E. A., Hagyard, M. J., and Smith, J. E.: 1980, *Bull. Am. Astron. Soc.* **12**, 476.